

Synchronous single-photon detection with GHz-gated superconducting nanowire detectors

E. Knehr,^{1,2,a)} A. Kuzmin,¹ S. Doerner,¹ S. Wuensch,¹ K. Ilin,¹ H. Schmidt,^{2,3} and M. Siegel¹

¹⁾*Institute of Micro- and Nanoelectronic Systems, Karlsruhe Institute of Technology (KIT), Karlsruhe, Germany*

²⁾*Leibniz Institute of Photonic Technology, Jena, Germany*

³⁾*Institute for Solid State Physics, Friedrich Schiller University Jena, Jena, Germany*

(Dated: 24 March 2020)

We demonstrate a GHz-gated operation of superconducting nanowire single-photon detectors suitable for synchronous applications. In comparison with conventional dc-biased nanowire detectors, this method prevents the detector from latching and can suppress dark counts and background noise. Using a gating frequency of 3.8 GHz and a fast, synchronized laser diode, we show that the detector's operation point follows the oscillating current and its detection efficiency depends on the relative frequency and phase of the bias and modulated optical signal. The obtained experimental results are in good agreement with simulations, showing that the duty cycle of a gated detector can be adjusted in a wide range in case of a pronounced saturation of the current-dependent detection efficiency. This operation mode could be suitable for applications such as quantum key distribution and time-of-flight laser ranging.

Superconducting nanowire single-photon detectors (SNSPDs) offer many advantages over competing single-photon detector technologies. Due to their outstanding performance in terms of detection efficiency up to mid-infrared,^{1,2} detection speed,^{3,4} and timing precision,⁵ they are the single-photon detector of choice for many applications such as optical communication,⁶ laser ranging,^{7,8} and spectroscopy.⁹

SNSPDs are usually operated in free-running mode. This is in contrast to single-photon avalanche diodes (SPADs), which require a gated operation to mitigate afterpulsing.¹⁰ However, in applications with known photon arrival time spans, a gated operation is beneficial since background noise can be suppressed and the signal-to-noise ratio (SNR) therefore improved. Additionally, gating the SNSPD using bias modulation can be used to prevent latching,¹¹ which allows for a stable operation.

A gated or quasi-gated approach for SNSPDs has been adopted by various groups. Akhlaghi *et al.* presented a gated mode at 625 MHz with a dc offset to increase the maximum count rate.¹² To prevent latching due to unwanted backscattering in laser ranging (LIDAR) applications, Zhang *et al.* showed a dc operation with periodical off-states using a programmed bias source.¹³ For the application in quantum key distribution (QKD) systems, an auto-reset system for SNSPDs using a voltage-comparator was shown.¹⁴ This way, blinding attacks on the detector could be identified.

A gated operation of SNSPDs in the GHz range can approach free-running mode since the temporal distance between the active states is in the range of timing jitter of practical SNSPD devices (less than 100 ps for an operation at 5 GHz). Furthermore, it should be possible to adjust the duty cycle for a gated operation with bias modulation by changing the current amplitude, since the intrinsic detection efficiency (IDE) of an SNSPD has an S-shaped bias dependence (seen as a sigmoidal count rate dependence $CR(I_b) \propto IDE$).

Consequently, the operation of an SNSPD with a saturated $CR(I_b)$ -dependence could be modified between free-running and gated mode according to the requirements of a particular application.

Here, we present a solely rf-biased, GHz-gated operation scheme for SNSPDs synchronized to a fast laser diode. For applications such as optical communications, QKD, and LIDAR, the operation mode of microwave-biased SNSPDs shown here could offer three main advantages over conventional SNSPDs: a reduction of dark counts, the mitigation of background noise, and the prevention of detector latching.

Conventional free-running SNSPDs are operated by applying a dc bias current I_b slightly below the switching current I_{sw} . When a photon is absorbed by the nanowire, a normal-conducting domain is formed and its high resistance can be detected as a voltage pulse along the nanowire. After the superconductive state is restored, the current through the nanowire recovers to its operation point.

As an alternative operation suitable for detector arrays, a frequency-division multiplexing scheme for SNSPDs was proposed.¹⁵ In this case, the nanowire is embedded in a lumped-element resonant circuit coupled to a common feed line and is biased by a microwave current I_{rf} at the resonant frequency f_r . A detector click damps the resonant circuit and therefore leads to an increased transmission coefficient $|S_{21}|$ on the readout line at f_r . The operation principle of these "radio-frequency" SNSPDs (RF-SNSPDs) is more thoroughly described in Ref. 16.

With this scheme, latching is prevented due to the ring-down time of the resonator and the fact that the oscillating current effectively resets the detector twice each period. Furthermore, the microwave bias generated by frequency synthesizers can be significantly more stable and is easier to filter than dc bias. The ring-down time and, thus, the maximum count rate of a single detector can be designed to fit the application. Previously, an RF-SNSPD array with a ring-down time of only few ns was demonstrated.¹⁵ The combined counting speed of an RF-SNSPD array can therefore be in the range of few GHz.

^{a)}Electronic mail: emanuel.knehr@kit.edu

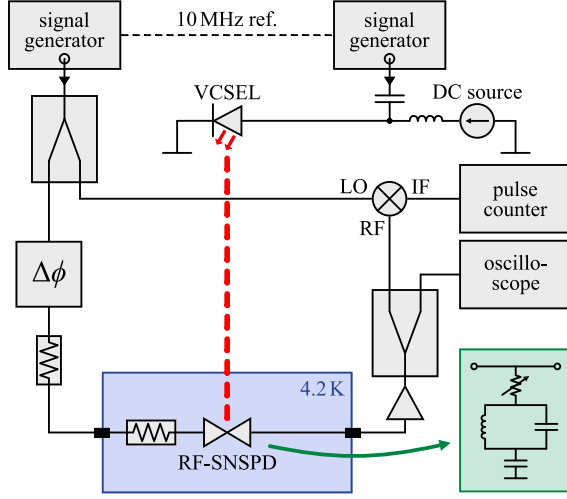


FIG. 1. Schematic of the experimental setup for synchronized photon detection. The RF-SNSPD (green rectangle) consists of the photon-sensitive nanowire, depicted here as a variable resistor, a resonant circuit defined by an inductor and a capacitor, and a coupling capacitor.

Due to the oscillating bias current and the sigmoidal bias dependence of IDE, the RF-SNSPD is not expected to be active all the time, i.e., in gated mode. In case of random photon arrival events (uniformly distributed in time), this should lead to a reduced detection efficiency compared to free-running SNSPDs operated at a dc bias equal to the amplitude of the rf current. For known photon arrival gates, on the other hand, the detection efficiency might be increased by synchronizing the oscillating IDE of the RF-SNSPD to the base clock of the optical signal in a way that their frequencies are related by a ratio of small integers.¹⁷ Here, we use the detector's rf bias signal oscillating with f_r to fully synchronize a modulated light source to the photon-sensitive time spans of the detector.

The RF-SNSPD used herein is fabricated from a 5 nm thick NbN layer, similar to those presented in Ref. 18, and is operated at its resonant frequency $f_r = 1.9$ GHz. Since the detection probability does not depend on the direction of the bias current, the intrinsic detection efficiency of the RF-SNSPD is expected to oscillate with the gating frequency f_g , which is twice the resonance frequency ($f_g = 2f_r$).

As a fast-switching light source, we use a vertical-cavity surface-emitting laser diode (VCSEL, Optek Technology OPV314YAT) emitting light at a wavelength of 850 nm and allowing for modulation frequencies $f_{\text{opt}} \lesssim 4.5$ GHz.

Two rf generators, which are phase-locked via a 10 MHz reference, provide the rf bias currents for both the laser diode and the RF-SNSPD (see Fig. 1). The laser diode is biased by a dc current of 3 mA and an rf current with an amplitude large enough to turn it off at the minimum, resulting in an optical output power modulated in the GHz range similar to on-off keying (OOK). To ensure a VCSEL modulation which resembles OOK, its signal was characterized using a fast photodiode (Thorlabs PDA8GS, DC–9.5 GHz). The RF-SNSPD is biased by an rf current only. The detector pulses are amplified by

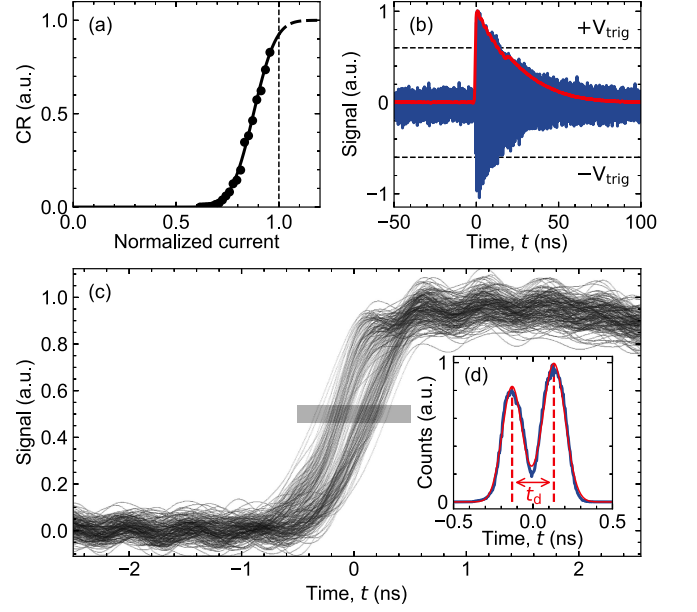


FIG. 2. Current-dependent count rate and traces of detector pulses over time. (a) Measured count rate dependent on the bias current normalized to the switching current. The line is a guide to the eye. (b) Single rf (blue) and downmixed (red envelope) pulse upon photon absorption. (c) Measured rising edge of multiple pulse envelopes. (d) Histogram of the normalized number of counts over time at the rising edge of the pulses (indicated by the semitransparent rectangle in (c)) with measurement in blue and Gaussian fits in red.

room-temperature amplifiers and read out by a 32 GHz real-time oscilloscope. Additionally, the rf pulses are downmixed by an analog mixer and the resulting envelope is read out with an ordinary pulse counter to measure count rates.

The current-dependent count rate of the detector is plotted in Fig. 2(a), without saturation up to the switching current.

In Fig. 2(b), a single detector response upon photon absorption and its envelope are shown. The decay time $\tau_d = Q_L / (\pi f_r) \approx 20$ ns is determined by the loaded quality factor Q_L of the resonant circuit. The detector investigated herein is part of a frequency-multiplexed detector array, for which the value $Q_L \approx 120$ was chosen to obtain a pixel frequency spacing in the range of several 10 MHz.

Figure 2(c) shows multiple traces of the envelope, which are obtained without synchronization to the optical source by triggering on the original rf pulse exceeding a defined zero-centered range ($-V_{\text{trig}}$ to $+V_{\text{trig}}$, see Fig. 2(b)). Two distinct groups of rising edges can be observed. This is also seen from the histogram of the number of counts, which is depicted in Fig. 2(d). The time difference between the two peaks amounts to $t_d \approx 263$ ps, which corresponds to a frequency $f \approx 3.8$ GHz or twice the resonance frequency.

The grouping of pulses shown in Fig. 2(c) is explained by the current-dependent count rate characteristic $CR(I_b)$ of the detector (Fig. 2(a)). In our particular experiment conducted at 4.2 K with 100 nm wide nanowires, the intrinsic detection efficiency does not reach 100% at 850 nm at any bias ampli-

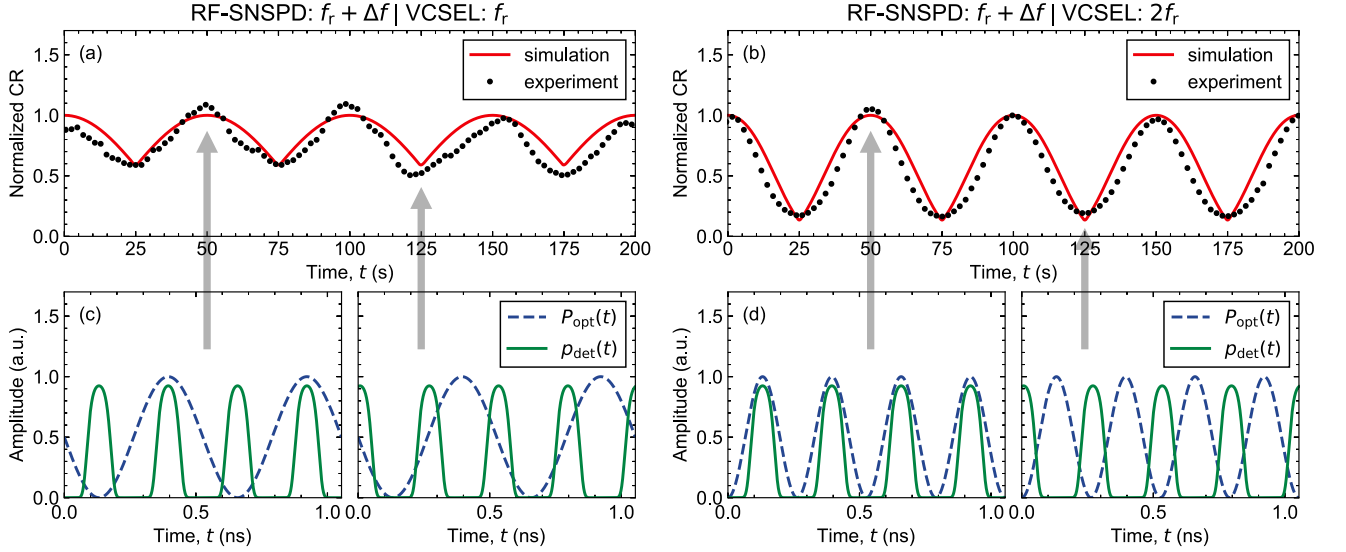


FIG. 3. Measurement and simulation of modulated count rate $CR(t)$ for a synchronized detection and beat frequency $\Delta f = 10$ mHz. (a), (b) Measurement and simulation of the modulated count rate CR over time. (c), (d) Simulation of the optical signal $P_{\text{opt}}(t)$ and the instantaneous detection probability $p_{\text{det}}(t)$ over time for operating frequencies $f_{\text{opt}}/f_r = 1$ and $f_{\text{opt}}/f_r = 2$, respectively. In each case, full alignment and misalignment between $P_{\text{opt}}(t)$ and $p_{\text{det}}(t)$ are depicted (corresponding to phases 0° and 180° of $p_{\text{det}}(t)$ relative to $P_{\text{opt}}(t)$ in (d)).

tude. Since the $CR(I_b)$ -curve is not saturated, the majority of the detection events will originate from bias points near the extrema ($\pm I_{\text{rf,max}}$). Therefore, a grouping of pulses is expected around these two bias points of opposite polarity. In other words, the two observed groups of traces correspond to two different phases of the bias current, separated by a phase shift of about 180° or half a period. This implies that the detector operation point oscillates with the gating frequency and the detector is active twice each period of the rf bias signal. The duration of the active states is defined as the time during which $|I_{\text{rf}}| \geq I_{\text{det}}$, with the minimal detection current I_{det} for a particular photon energy.

In order to show that the RF-SNSPD's detection efficiency depends on the relative phase of the rf bias and the optical signal, the phase-sensitive changes of the count rate are investigated. The measurements are conducted with the light modulated either with the resonance frequency of the RF-SNSPD ($f_{\text{opt}}/f_r = 1$) or with its gating frequency ($f_{\text{opt}}/f_r = 2$). To slowly sweep the relative phase of the signals, the frequency of the detector bias is detuned with respect to the modulation frequency of the laser diode by $\Delta f = 10$ mHz. This small detuning ($\Delta f/f_r \approx 10^{-12}$) should lead to a slow periodic modulation of the count rate with the beat frequency.

The phase-sensitive detection efficiency was analyzed experimentally (Fig. 3(a) and (b)) and oscillations of the count rate with a period of 50s are indeed visible. The measured count rate modulation indices $m = (CR_{\text{max}} - CR_{\text{min}})/(CR_{\text{max}} + CR_{\text{min}})$ amount to $m \approx 0.30$ and $m \approx 0.71$ for the case $f_{\text{opt}}/f_r = 1$ and $f_{\text{opt}}/f_r = 2$, respectively. The modulation period of 50s observed for a detuning $\Delta f = 10$ mHz corresponds to a detuning $\Delta f_g = 20$ mHz in gating frequency, which is in accordance with the result in Fig. 2(d).

To describe the obtained data, we simulate the temporal de-

pendence of the count rate by means of simple models of the operation conditions. For this, we take a sinusoidal rf bias current

$$I_{\text{rf}}(t) = \sin[(\omega_r + \Delta\omega)t], \quad (1)$$

with $\omega_r = 2\pi f_r = 2\pi \times 1.9$ GHz and $\Delta\omega = 2\pi\Delta f = 2\pi \times 10$ mHz. The instantaneous detection probability $p_{\text{det}}(t)$ is then estimated from the measured current dependence of the intrinsic detection efficiency (Fig. 2(a)) by fitting

$$p_{\text{det}}(t) = a \left[1 + \text{erf} \left(\frac{|I_{\text{rf}}(t)| - c}{b} \right) \right] \quad (2)$$

to the experimental $CR(I_b)$ -curve with the fitting parameters a for probability normalization, b for the transition width of the $CR(I_b)$ -curve, and c for the bias corresponding to a detection probability of 50% (related to the minimal detection current I_{det} for photons of 850nm wavelength). Since $p_{\text{det}}(t)$ in Eq. 2 depends on the modulus of the rf bias $|I_{\text{rf}}| \propto \sqrt{1 - \cos(2\omega_r t)}$, it oscillates with the frequency $f_g = 2f_r$.

The harmonic, amplitude modulated optical signal is modelled by

$$P_{\text{opt}}(t) = P_{\text{max}} (1 + \cos \omega_{\text{opt}} t) / 2, \quad (3)$$

with the modulation frequency of the laser diode $\omega_{\text{opt}} = 2\pi f_{\text{opt}}$ and a peak optical power P_{max} absorbed in the detector. Both the instantaneous detection probability $p_{\text{det}}(t)$ and the normalized optical power $P_{\text{opt}}(t)$ are plotted over time in Fig. 3(c) and (d) for operation frequencies $f_{\text{opt}}/f_r = 1$ and $f_{\text{opt}}/f_r = 2$, respectively.

The expected time-dependent count rate amounts to

$$CR(t) = \frac{1}{E_{\text{ph}} \tau} \int_0^\tau p_{\text{det}}(t) \cdot P_{\text{opt}}(t) dt, \quad (4)$$

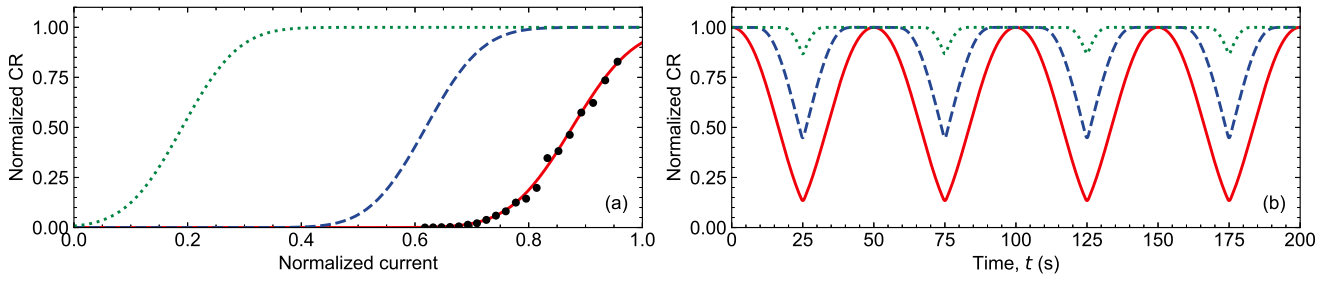


FIG. 4. Simulation of different $CR(I_b)$ -curves (a) and their corresponding modulated $CR(t)$ according to Eq. 4 for $f_{\text{opt}}/f_r = 2$ (b). The black dots in (a) indicate measurement results. The solid, red curves represent the conditions of Fig. 3(b).

with the collection time $\tau = 1$ s. A comparison of the simulated and measured count rate $CR(t)$ can be seen in Fig. 3(a) and (b). As indicated by the arrows, the maxima and minima of $CR(t)$ correspond to detector gates fully aligned and misaligned to the optical pulses.

The measurement data coincide quite well with the simulated curves both in beat frequency and modulation index m . The larger modulation index for $f_{\text{opt}}/f_r = 2$, in which case the detector and the laser diode are operated with the same frequency and phase, signifies that the detection efficiency can be increased significantly by synchronizing the detector to the light source. The attenuation of stray light and suppression of dark counts can be quantified by the factor $(1+m) \cdot (1-m)^{-1}$, with a value of about 6.0 for $f_{\text{opt}}/f_r = 2$.

According to our simple model, the duty cycle of the gated detector and therefore the modulation index of $CR(t)$ is highly dependent on the $CR(I_b)$ -characteristic of the detector. With a non-saturated $CR(I_b)$ -curve, the investigated detector exhibits a gated detection with photon detection mainly occurring for a current I_{rf} near the extrema $\pm I_{\text{rf,max}}$, as discussed before (see solid, red curves in Fig. 4). In case of a pronounced count rate plateau, however, the active time spans can be much longer and the detection is less dependent on the relative phase of the optical signal $P_{\text{opt}}(t)$. This is simulated for two saturated $CR(I_b)$ -curves (see dashed and dotted curves in Fig. 4). For a broader saturation in Fig. 4(a), the corresponding modulation of $CR(t)$ seen in Fig. 4(b) is much smaller, with decreasing modulation indices m of 0.75, 0.4, and 0.1, respectively. In the latter case, the pure rf bias leads only to a slightly decreased detection efficiency in case of random photon arrival times and therefore becomes comparable to free-running mode. Thus, the duty cycle of an RF-SNSPD with a pronounced count rate saturation can be tuned between gated and quasi-free-running mode by choosing an appropriate rf bias amplitude.

In conclusion, we have shown a latching-free GHz-gated operation of resonator-coupled SNSPDs, which can approach free-running detectors. The detector is biased by a microwave current and its operation point is modulated accordingly. Synchronous measurements indicate an instantaneous intrinsic detection efficiency following the rf bias current, which agrees well with our simple model of the phase-sensitive count rate. That way, we showed that the detection efficiency of RF-SNSPDs can be maximized and the influence of stray light

minimized by using a phase-locked light modulation with a frequency twice the rf bias frequency. The duty cycle of the detector can be much larger for devices demonstrating a pronounced plateau in the current dependence of the detection efficiency. In this case, the photon count rate of an RF-SNSPD is not degraded significantly even in asynchronous mode, which sets it on par with dc-biased free-running SNSPDs. Moreover, count rates in GHz range are possible using a frequency-multiplexed detector array of RF-SNSPDs with moderate Q factors. Hence, a gated single-photon detection with a total data rate of few Gbit/s could be achievable.

- ¹F. Marsili, F. Bellei, F. Najafi, A. E. Dane, E. A. Dauler, R. J. Molnar, and K. K. Berggren, *Nano Lett.* **12**, 4799 (2012).
- ²F. Marsili, V. B. Verma, J. A. Stern, S. Harrington, A. E. Lita, T. Gerrits, I. Vayshenker, B. Baek, M. D. Shaw, R. P. Mirin, and S. W. Nam, *Nat. Photonics* **7**, 210 (2013).
- ³A. J. Kerman, E. A. Dauler, W. E. Keicher, J. K. W. Yang, K. K. Berggren, G. Gol'tsman, and B. Voronov, *Appl. Phys. Lett.* **88**, 111116 (2006).
- ⁴S. Ferrari, V. Kovalyuk, A. Vetter, C. Lee, C. Rockstuhl, A. Semenov, G. Gol'tsman, and W. Pernice, *Appl. Phys. Lett.* **115**, 101104 (2019).
- ⁵B. Korzh, Q.-Y. Zhao, J. P. Allmaras, S. Frasca, T. M. Autry, E. A. Bersin, A. D. Beyer, R. M. Briggs, B. Bumble, *et al.*, *Nat. Photonics* (2020).
- ⁶M. Shaw, F. Marsili, A. Beyer, R. Briggs, J. Allmaras, and W. H. Farr, *Proc. SPIE* **10096**, 100960J (2017).
- ⁷A. McCarthy, N. J. Krichel, N. R. Gemmill, X. Ren, M. G. Tanner, S. N. Dorenbos, V. Zwiller, R. H. Hadfield, and G. S. Buller, *Opt. Express* **21**, 8904 (2013).
- ⁸H. Li, S. Chen, L. You, W. Meng, Z. Wu, Z. Zhang, K. Tang, L. Zhang, W. Zhang, X. Yang, X. Liu, Z. Wang, and X. Xie, *Opt. Express* **24**, 3535 (2016).
- ⁹L. Chen, D. Schwarzer, J. A. Lau, V. B. Verma, M. J. Stevens, F. Marsili, R. P. Mirin, S. W. Nam, and A. M. Wodtke, *Opt. Express* **26**, 14859 (2018).
- ¹⁰J. Zhang, M. A. Itzler, H. Zbinden, and J.-W. Pan, *Light Sci. Appl.* **4**, e286 (2015).
- ¹¹A. J. Kerman, J. K. W. Yang, R. J. Molnar, E. A. Dauler, and K. K. Berggren, *Phys. Rev. B* **79**, 100509 (2009).
- ¹²M. K. Akhlaghi and A. H. Majedi, *Opt. Express* **20**, 1608 (2012).
- ¹³L. Zhang, S. Zhang, X. Tao, G. Zhu, L. Kang, J. Chen, and P. Wu, *IEEE Trans. Appl. Supercond.* **27**, 1 (2017).
- ¹⁴M. Elezov, R. Ozhegov, G. Goltsman, and V. Makarov, *Opt. Express* **27**, 30979 (2019).
- ¹⁵S. Doerner, A. Kuzmin, S. Wuensch, K. Ilin, and M. Siegel, *IEEE Trans. Appl. Supercond.* **26**, 1 (2016).
- ¹⁶S. Doerner, A. Kuzmin, S. Wuensch, I. Charaev, and M. Siegel, *IEEE Trans. Appl. Supercond.* **27**, 1 (2017).
- ¹⁷S. Doerner, A. Kuzmin, S. Wuensch, and M. Siegel, *IEEE Trans. Appl. Supercond.* **29**, 1 (2019).
- ¹⁸S. Doerner, A. Kuzmin, S. Wuensch, I. Charaev, F. Boes, T. Zwick, and M. Siegel, *Appl. Phys. Lett.* **111**, 032603 (2017).